ARTICLE

Theoretical Study on Mechanism and Kinetics of Reaction of O(^{3}P) with Propane

Fu-qiang Jing[a,b], Jian-wei Cao[b], Xiao-jun Liu[a], Yu-feng Hu[a], Hai-tao Ma[b*], Wen-sheng Bian[b,c*]

a. Key Laboratory of Luminescence and Optical Information, Ministry of Education, Beijing Jiaotong University, Beijing 100044, China
b. Beijing National Laboratory for Molecular Sciences, Institute of Chemistry, Chinese Academy of Sciences, Beijing 100190, China
c. University of Chinese Academy of Sciences, Beijing 100049, China

(Dated: Received on March 7 2016; Accepted on April 29, 2016)

The reaction of C_3H_8+O(^{3}P)→C_3H_7+OH is investigated using *ab initio* calculation and dynamical methods. Electronic structure calculations for all stationary points are obtained using a dual-level strategy. The geometry optimization is performed using the unrestricted second-order Møller-Plesset perturbation method and the single-point energy is computed using the coupled-cluster singles and doubles augmented by a perturbative treatment of triple excitations method. Results indicate that the main reaction channel is C_3H_8+O(^{3}P)→*i*-C_3H_7+OH. Based upon the *ab initio* data, thermal rate constants are calculated using the variational transition state theory method with the temperature ranging from 298 K to 1000 K. These calculated rate constants are in better agreement with experiments than those reported in previous theoretical studies, and the branching ratios of the reaction are also calculated in the present work. Furthermore, the isotope effects of the title reaction are calculated and discussed. The present work reveals the reaction mechanism of hydrogen-abstraction from propane involving reaction channel competitions is helpful for the understanding of propane combustion.

Key words: Reaction mechanism, Thermal rate constant, Variational transition state theory, Isotope effect

I. INTRODUCTION

Recently, with the sharp increase of the number of traditional fuel vehicle, the vehicle tail gas exhaust has led to some severe issues to human health and global environment. Liquefied petroleum gas (LPG) fuel, mainly consisting of propane and *n*-butane, is widely used as green fuel in engine due to its little exhaust producing [1]. In addition, LPG can be further separated and purified to produce pure propane, which can be used as general engine fuel and potential fuel of turbine engine [2]. Therefore, the study on the combustion reaction of propane is of considerable current interest.

The combustion process of propane involves many kinds of chemical reaction, in which the hydrogen-abstraction reaction of propane with O(^{3}P) is the most important. Experimentally, the previous studies on the hydrogen-abstraction reaction of propane were mainly focused on the product branching ratio and rate constant [3−8]. In the early 1970s, McLain *et al.* studied the rate constants of hydrogen-abstraction reaction of propane with the shock wave [3]. In 1981, Jewell *et al.* measured the rate constants of the hydrogen-abstraction reaction of propane both by the measurement of O-atom decay in the presence of excess propane and by measuring the change in propane concentration after an appropriate time in the presence of an excess of oxygen atoms [4]. In 1991, Cohen and Westberg measured the rate constant of C_3H_8+O(^{3}P)→C_3H_7+OH reaction at 298 K and reported a value of 6.6×10^{-15} cm^3/(molecule·s) [5]. In 1994 and 1996, Miyoshi *et al.* [6, 7] studied the C_3H_8+O(^{3}P) reaction using the laser photolysis-photoionization mass spectrometer and laser photolysis-shock tube, and measured the site-specific branching fractions at 593, 944, and 1130 K, respectively.

On the other hand, very limited theoretical studies on the C_3H_8+O(^{3}P) reaction has been reported, and a detailed research on the mechanism of this hydrogen-abstraction reaction is still lacking. In 2004, Troya *et al.* obtained the reaction barrier height using density functional theory method [9]. In 2007, Troya *et al.* obtained the thermal rate constants at 298 K using the transition-state theory (TST) method for the title reaction based upon the second-order Møller-Plesset perturbation theory (MP2) with the aug-cc-pVDZ basis

*Authors to whom correspondence should be addressed. E-mail: mht@iccas.ac.cn, bian@iccas.ac.cn

sets [10].Up to now, few studies on the isotope effects of the title reaction has been reported.

In this work, the *ab initio* and dynamical methods are used to study the hydrogen-abstraction reaction of C_3H_8+O(^{3}P). The main reaction channel is determined and the reaction rate constants are calculated, and the obtained results are in good agreement with the available experimental data and superior to the previous theoretical results. The kinetic isotope effects are also studied and discussed.

II. COMPUTATIONAL DETAILS AND METHODS

The unrestricted second-order Møller-Plesset perturbation (UMP2) method is used to fully optimize the equilibrium geometries of various stationary points of the title reaction with the correlation-consistent triple-ϵ basis set of Dunning augmented with diffuse functions (aug-cc-pVTZ) basis set. The intrinsic reaction coordinate (IRC) [11, 12] calculations are carried out to confirm the transition states (TSs) connecting the right minima [13−15]. To obtain more accurate energies, the dual-level strategy is employed. The details of the dual-level strategy can be found elsewhere and only a brief outline will be given here [16]. The idea of the dual-level strategy is to use two levels of *ab initio* calculations so as to reduce the number of high-level points needed. The final single-point energies for all the points on the IRC are evaluated at coupled-cluster singles and doubles augmented by a perturbative treatment of triple excitations (CCSD(T)) with aug-cc-pVQZ level. All *ab initio* calculations reported in the present work are performed using the Gaussian 09 suite of *ab initio* programs [17].

The variational transition state theory calculations are carried out using the POLYRATE2015 program [18]. All coordinates are scaled to a reduced mass. The reaction path is calculated with sufficiently small step size by the Euler steepest-descent method from the TS geometry and goes downhill to both the asymptotic reactant and product channels. Cartesian coordinates are used to parameterize the reaction path. The rate constants reported here are those obtained from the microcanonical variational theory (μVT) calculations [19]. The μVT is based on the idea of minimizing the microcanonical rate constants along the minimum energy path (MEP), which can minimize the error caused by the "recrossing" trajectories [19]. Within the framework of μVT, the rate constant at a fixed temperature T can be expressed as:

$$k^{\mu VT}(T) = \frac{\int_0^\infty \min\left[N^{GTS}(E,s)\right] e^{-E/k_B T} dE}{h\Phi^R} \quad (1)$$

where Φ^R is the total reactant partition function, which is the product of electronic, rotational, and vibrational partition functions. The relative translational partition function is calculated classically and is included in Φ^R. However, the rotational and vibrational partition functions of the reactant are calculated quantum mechanically within the rigid rotor and harmonic oscillator approximations, respectively. $N^{GTS}(E,s)$ is the sum of states of electronic, rotational, and vibrational motions at energy E of the generalized transition state located at the reaction coordinate s.

In addition, the quantum-tunneling effects are accounted for by the multidimensional small-curvature-tunneling (SCT) transmission coefficient [20]. The rate constants reported here are those obtained from the μVT with the SCT transmission coefficient calculations.

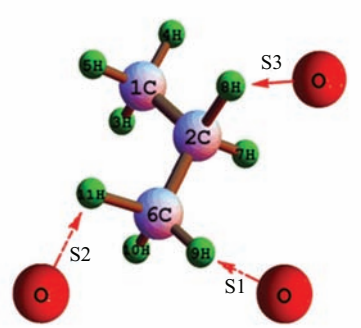

FIG. 1 Schematic of the oxygen attacking spots (S1, S2, and S3) in hydrogen-abstraction reaction of C_3H_8+O(^{3}P)→C_3H_7+OH. The red atoms are oxygen atoms, the green atoms are hydrogen atoms, and others are carbon atoms.

III. RESULTS AND DISCUSSION

A. Investigation for main reaction channel in the hydrogen-abstraction of O(^{3}P)+C_3H_8

Figure 1 shows the effective sites (denoted with S1, S2, and S3, respectively) of the O(^{3}P) atom attacking in the title reaction. As shown in the Fig.1, S1 corresponds to the H atoms located in the plane of the carbon atoms. Both the TS and *n*-propyl radical produced by hydrogen abstraction at this site possess C_s symmetry. The second site S2 corresponds to the H atom out-of-plane atoms, and the TS and *n*-propyl radical are not symmetric. The TS and isopropyl radical corresponding to the site S3 are C_s-symmetric. Eventually, there are two final products formed at these three sites in the hydrogen-abstraction reaction of propane with O(^{3}P), namely *n*-propyl and *i*-propyl: $CH_3CH_2CH_3$+O(^{3}P)→*n*-C_3H_7+OH or *i*-C_3H_7+OH.

Having depicted these three attacked sites, we are endeavoring to explore the main reaction channel. The first step is to locate the stationary points [21, 22]. As shown in Fig.2, for each channel, five stationary points (the reactants, TSs, products, and two van der Waals (vdW) wells) [23] are optimized at the UMP2/aug-cc-pVTZ level [24, 25] to characterize the core reactivity parameters of the title reaction. The path 1,

DOI:10.1063/1674-0068/29/cjcp1603042

path 2, and path 3 correspond to the different channels of hydrogen-abstraction locations S1, S2, and S3 respectively. It should be noted that the product energies of the n1-C_3H_7 and n2-C_3H_7 channel have small difference due to variation of the dihedral angle. In the hydrogen-abstraction reaction process, the barrier for the channel of $C_3H_8+O(^3P)\rightarrow i$-$C_3H_7$+OH is much lower than that for the channels of $C_3H_8+O(^3P)\rightarrow n$1-$C_3H_7$+OH and $C_3H_8+O(^3P)\rightarrow n$2-$C_3H_7$+OH, indicating that $C_3H_8+O(^3P)\rightarrow i$-$C_3H_7$+OH is the main reaction channel. Additionally, since the difference between the total spin value before annihilation and the theoretical value is within 2%, the spin contamination can be ignored.

Moreover, for each channel of the title reaction, there is a vdW well in the entrance valley, which is caused by the dispersion force between non-polar $O(^3P)$ atom and polar propane molecule; there is also a relative deep vdW well in the exit valley, which is caused by the strong force between permanent dipoles, C_3H_7 and OH radical. These vdW complexes may play an important role in the detailed reaction dynamics [26]. For each channel, the energy difference value of vdW wells in the entrance and exit valleys is very obvious. Especially for the main channel, the energy of vdW well in the entrance and exit valleys are 0.6 kcal/mol (relative to the energy of reactant) and 4.6 kcal/mol (relative to the energy of product) respectively. In addition, bases set superposition errors (BSSEs) are taken into account for vdW wells, the corrected vdW well depths in the entrance valleys are 0.4 kcal/mol (path 1), 0.6 kcal/mol (path 2), and 0.5 kcal/mol (path 3), respectively. As for the vdW wells in the exit valleys, the corrected well depths are 3.5 kcal/mol (path 1), 3.6 kcal/mol (path 2), and 4.3 kcal/mol (path 3), respectively. The magnitudes of BSSEs for the vdW wells in the entrance and exit valleys are very small.

The optimized geometries of various reactants, products, TSs and vdW wells in three reaction channels are obtained at UMP2/aug-cc-pVTZ level, as shown in Table I. The reaction energies and imaginary frequencies for three TSs (denoted TS1, TS2, and TS3, respectively) are also compared. The imaginary frequencies (TS1: 2071i, TS2: 2053i, TS3: 1897i cm^{-1}) are consistent with the result obtained by Troya (2048i, 2025i, 1891i cm^{-1}). And the imaginary frequency for TS3 (1897i cm^{-1}) is more than 100 cm^{-1} smaller than both of other two, which indicates that i-propyl+OH path is much less sharply peaked in the TS region than n-propyl+OH path. Regarding the barrier energy, the barrier energy for hydrogen abstraction at S3 site (11.6 kcal/mol) is more than 2.0 kcal/mol lower than S1 (14.1 kcal/mol) and S2 (13.6 kcal/mol) sites, which is in agreement with the trend observed in experiment through determining the activation energy values [27]. This result also highlights the Troya's result: the reaction barriers in the hydrogen-abstraction reactions of $C_3H_8+O(^3P)$ are in the primary>secondary

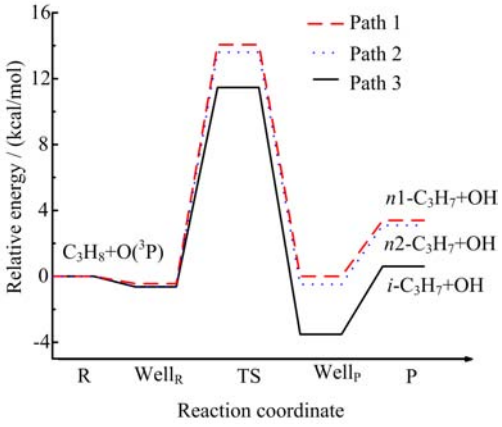

FIG. 2 Detailed schematic of the three reaction channels of the hydrogen-abstraction reaction of propane with $O(^3P)$. The relative energies are computed by taking the energy of reactants as zero. The stationary points of reactant (R), van der Waals wells of the reactant side well (Well$_R$) and the product side well (Well$_P$), transition state (TS) and product (P) are described in detail.

order. In addition, the zero-point corrected values of reaction barriers for the abstraction at S1, S2, and S3 sites calculated by CCSD(T)/aug-cc-pVQZ level are 10.3, 10.0, and 7.9 kcal/mol respectively, and the basis set level is higher than Troya's (aug-cc-pVTZ). Moreover, for the products of $C_3H_8+O(^3P)\rightarrow C_3H_7$+OH reaction, the forming bond (O−H) length is 0.960 Å in path 3, 0.975 Å in path 1 and path 2, and these three different breaking bonds (C−H) length becomes longer from reactants (1.104 Å in path 3, 1.101 Å in path 1, 1.103 Å in path 2) in the reaction. While the other C−H bonds length and C−C bonds length are almost unchanged in the entire reaction paths. For the TS geometries, the forming bond (O−H) and the breaking bond (C−H) are respectively 2.5% longer and 1.3% shorter in path 3 than that in path 1 and path 2. Therefore, electronic structure calculations indicate that the TS for hydrogen-abstraction at S3 site is more reactant-like than that at S1 and S2 sites.

B. The reaction mechanism of $C_3H_8+O(^3P)$

For further investigating the reaction mechanism, it is desirable to find a connecting pathway among these stationary points (reactants, TSs, products, and vdW wells) on the potential energy surface. This pathway is defined as the steepest descent path from the TS to the minima and is found in mass-weighted cartesian coordinates [11, 28, 29]. The MEPs are affirmed by IRC calculation in Fig.3. For the following kinetic calculations, the energies, gradients, and hessian matrix of the points on IRC (101, 110, 87 points for path 1, path 2, path 3, respectively) are necessary. The IRC is smooth and reasonable, which confirms the reliability of the calculations. As shown in Fig.3, the energy of products is

DOI:10.1063/1674-0068/29/cjcp1603042

TABLE I Calculated characteristic geometrical parameters and energies of various stationary point in C_3H_8+O(^{3}P)→ C_3H_7+OH reaction

Path			Reactant	vdW well		TS		Product
				$Well_R$	$Well_p$	This work	Ref.[10]	
Path 1	E^a/(kcal/mol)		0	−0.4	−3.6[b]	14.1		4.9
	ω_i[c]/cm^{-1}					2071	2048	
	Bond length/Å	O−9H		2.989	0.982	1.254	1.253	0.975
		6C−9H	1.101	1.101	2.213	1.246	1.246	
		6C−11H	1.103	1.103	1.093	1.099		1.092
		3C−10H	1.103	1.103	1.093	1.099		1.091
		2C−1C	1.533	1.533	1.547	1.538		1.546
		2C−6C	1.533	1.533	1.501	1.518		1.499
	Angle/(°)	1C−9H−O		129.3	174.7	177.8	177.8	
		2C−6C−9H	111.7	111.5	97.2	108.2		120.7
		1C−2C−6C	112.1	112.1	111.8	111.2		112.4
	Dihedral angle/(°)	O-6C−2C−1C		179.9	179.9	−179.9		
		9H−6C−2C−1C	179.9	−180.0	179.9	−179.9		
		10H−6C−2C−1C	−59.9	−59.7	−80.2	−65.6		84.2
		11H−6C−2C−1C	59.9	59.7	80.0	65.3		−84.3
Path 2	E^a/(kcal/mol)		0	−0.6	−3.8[b]	13.6		4.6
	ω_i[c]/cm^{-1}					2053	2025	
	Bond length/Å	O−11H		3.085	0.975	1.259	1.259	0.975
		6C−11H	1.103	1.102	2.194	1.245	1.245	
		6C−10H	1.103	1.103	1.094	1.099		1.092
		6C−9H	1.101	1.102	1.093	1.099		1.091
		2C−1C	1.533	1.533	1.535	1.533		1.546
		2C−3C	1.533	1.533	1.500	1.519		1.499
	Angle/(°)	1C−11H−O		123.1	173.2	176.9	176.9	
		2C−6C−11H	110.8	110.6	95.8	107.2		120.5
		1C−2C−6C	112.1	112.0	112.9	112.3		112.8
	Dihedral angle/(°)	O−6C−2C−1C		79.9	67.4	62.6		
		9H−6C−2C−1C	−179.9	179.8	164.9	175.8		−162.3
		10H−6C−2C−1C	−59.7	−59.9	−33.2	−51.9		28.1
		11H−6C−2C−1C	59.7	59.6	66.4	61.8		
Path 3	E^a/(kcal/mol)		0	−0.6	−4.6[b]	11.6		2.5
	ω_i[c]/cm^{-1}					1897	1891	
	Bond length/Å	O−8H		3.038	0.983	1.287	1.288	0.960
		2C−8H	1.104	1.103	2.136	1.229	1.228	
		2C−7H	1.104	1.104	1.094	1.107		1.122
		2C−1C	1.533	1.533	1.500	1.520		1.507
		2C−3C	1.533	1.533	1.500	1.520		1.507
	Angle/(°)	2C−8H−O		116.2	170.9	177.4	174.2	
		7H−2C−8H	106.5	106.7	99.8	101.8		
		1C−2C−3C	112.1	112.0	119.4	115.5		111.8
	Dihedral angle/(°)	O−2C−1C−6C		−80.3	−96.9	−116.3		
		7H−2C−1C−6C	121.8	121.8	156.5	131.8		110.1
		8H−2C−1C−6C	−121.8	−121.5	−99.4	−117.5		

[a] Energies are computed by taking the energy of reactants as zero.
[b] Energies are relative to the energy of products.
[c] ω_i is the imaginary frequency.

DOI:10.1063/1674-0068/29/cjcp1603042

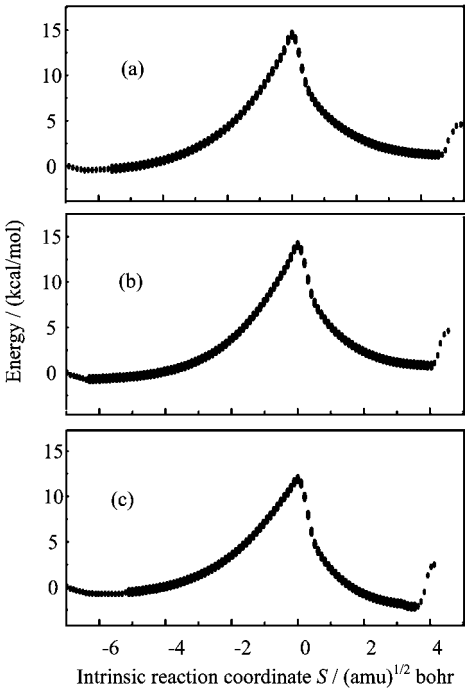

FIG. 3 C_3H_8+O(^{3}P) reaction paths obtained at the UMP2/aug-cc-pVTZ level for S1, S2 and S3. The energies are relative to the energy of reactants. (a) Path 1, (b) path 2, (c) path 3.

higher than the energy of reactants, hence the reaction turns out to be endothermic as a whole. These channels can be divided into three regions: the association region is from reactants to vdW potential well, the abstraction region is from vdW potential well to the potential well of product side through TS, the dissociation region is from the potential well of product side to products. The mechanism of the hydrogen-abstraction reaction on the IRC can be explained as follows. For each channel, initially the O(^{3}P) atom attacks one of the H atoms in C_3H_8 molecule, leading to a collision complex, which is a very fast step with the energy releasing. And then the bond between attacked H and O(^{3}P) atom forms. At last, the bond between attacked H and C atom breaks, leading to the formation of products (C_3H_7+OH) via the TS.

C. The thermal reaction rate constants of C_3H_8+O(^{3}P) →C_3H_7+OH

The reaction channel C_3H_8+O(^{3}P)→*i*-C_3H_7+OH has a single saddle point (typical for the TST), and consequently, the TST and μVT methods were applied in this case. These calculations are based upon dual-level strategy extensive electronic structure determinations. According to the geometries, harmonic frequencies, and energy of reactants, products and TSs, the thermal rate constants of the main reaction channel have been calculated at different temperature ranging from 298 K to 1000 K, which are plotted in Fig.4 as a typical Arrhenius behaviour. The calculated rate constants for C_3H_8+O(^{3}P)→C_3H_7+OH reaction are 3.43×10^{-15}, 1.46×10^{-11}, 1.54×10^{-11}, 1.63×10^{-11} cm^3/(molecule·s) at 298, 939, 946, and 957 K by using μVT/SCT method. The value of the rate constant at 298 K is in better agreement with the experimental result (6.6×10^{-15} cm^3/(molecule·s) [5] than that from Troya's calculation (9.60×10^{-16} cm^3/(molecule·s) [10]. Besides, these calculated rate constant values at 939, 946, and 957 K are also in good agreement with the experimental results (8.44×10^{-12}, 5.80×10^{-12}, 7.63×10^{-12} cm^3/(molecule·s) obtained by Miyoshi *et al.* [6], respectively. In addition, the branching ratios (k_n/k_i) are calculated at 593, 944, and 1130 K, respectively. And the obtained values (0.35, 0.72, 0.88) are in good agreement with the experimental values (0.41, 0.80, 0.92) [7]. The remaining discrepancy between the experimental and present theoretical values may be because there is some uncertain factors in the experiments [20, 29, 30]. We also find that at low temperatures, the effect of tunneling on rate constants is obvious, and the correction of tunneling effect is necessary [16]. For instance, tunnelling accounts for about 91% of reaction rate constant at 298 K, and proportion decreases to 18% at 1000 K. The comparison with previous theoretical calculation as well as the experimental measurements is also shown in Fig.4. It is encouraging to see that our results are in good agreement with the experimental values within limits of error. And the μVT/SCT calculation results are closer to the experimental results than μVT calculation results, which indicates that the tunneling effect plays an important role in rate constants. The result estimated by SCT method is improved significantly.

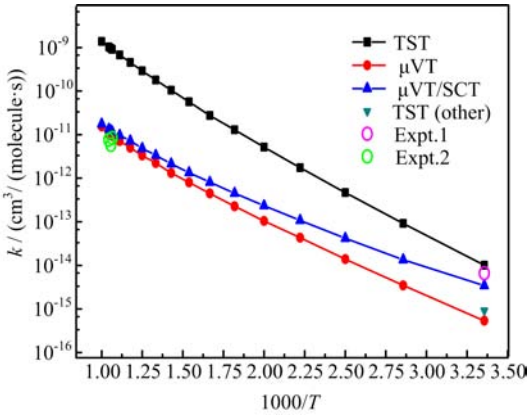

FIG. 4 Arrhenius plot for the reaction of C_3H_8+O(^{3}P)→C_3H_7+OH. TST: present study TST calculation, μVT: present study using μVT calculation, μVT/SCT: present study using μVT with SCT calculation, TST (other) from Ref.[10], Expt.1: experimental data from Ref.[5], Expt.2: experimental data from Ref.[6].

DOI:10.1063/1674-0068/29/cjcp1603042

D. The kinetic isotope effects for C_3H_8+O(^{3}P) →*i*-C_3H_7+OH

Following the calculation for the reaction rate constants of C_3H_8+O(^{3}P)→*i*-C_3H_7+OH, we perform a study for isotopic substitution effect. It is well known that the change of isotope will affect rate constants, which can also provide vital clues for reaction pathways. Generally, isotopic substitution occurs in an atom that participates in the reaction, which will produce the primary isotope effect; if the isotopic substitution is made with an atom that does not take part in the reaction directly, a secondary isotope effect will be produced [31].

In our study, these two isotope effects are both considered in the hydrogen-abstraction reaction of C_3H_8+O(^{3}P)→*i*-C_3H_7+OH. As shown in Fig.5, all the rate constants are calculated using TST and μVT methods. And the quantum-tunneling effects are also estimated by SCT method. For the first case (Fig.5(a)), the H atom that participates in the reaction directly is replaced by D atom, C_3H_7D+O(^{3}P)→*i*-C_3H_7+OD (R1), and there is only the primary isotope effect. Compared with the rate constants of C_3H_8+O(^{3}P) reaction, the obtained rate constants with primary isotope effect are lower. For the second case (Fig.5(b)), where all H atoms in propane molecule are substituted by D atoms, C_3D_8+O(^{3}P)→*i*-C_3D_7+OD (R2), the primary and secondary isotope effects coexist in the hydrogen-abstraction reaction. From the Fig.5(b), we notice that the reaction rate constants with the secondary isotope effect are lower than that with only the primary isotope effect.

Comparing the above reaction rate constants, we notice that rate constants with isotope effects are all lower than C_3H_8+O(^{3}P)→*i*-C_3H_7+OH reaction. This may result from that the C−D bond has a lower zero-point energy than the C−H bond and a higher activation energy for bond breaking is therefore required. We also find that the primary isotope effect is the main impact of the rate constants. This is because that the atom substituted by isotopic atom does not directly participate in the reaction, and extra activation energy for bond breaking is not needed.

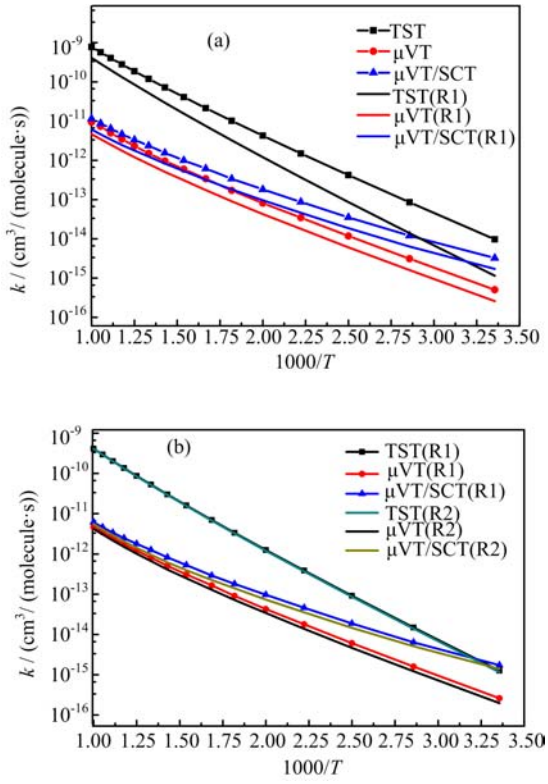

FIG. 5 Arrhenius plot for the isotope effects on the rate constants. R1: H atom, which is directly participate in the reaction, substituted by D atom, C_3H_7D+O(^{3}P)→*i*-C_3H_7+OD. R2: all H atoms in propane molecule substituted by D atoms, and secondary isotope effect exists, C_3D_8+O(^{3}P)→*i*-C_3D_7+OD. (a) Comparing the results of TST, μVT, μVT/SCT, and TST(R1), μVT(R1), μVT/SCT(R1). (b) Comparing the results of TST(R1), μVT(R1), μVT/SCT(R1), and TST(R2), μVT(R2), μVT/SCT(R2). TST: present study TST calculation. μVT: present study μVT calculation. μVT/SCT: present study μVT with SCT calculation.

IV. CONCLUSION

We have used the *ab initio* and dynamical methods to compute the rate constants, and investigated the path energy and reaction barriers of the hydrogen-abstraction reactions between O(^{3}P) atom and propane molecule. Among, the reaction barriers for title abstraction reaction are calculated by using a dual-level strategy. We find out three channels and determine the lowest barrier channel (C_3H_8+O(^{3}P)→*i*-C_3H_7+OH) in this reaction. This theoretical research on the typical reaction reveals the characteristics of the propane combustion reaction, which provides a theoretical support for the accurate measurements of the combustion intermediates and final products. The vdW wells found in this work are expected to play an important role in more detailed dynamical studies. Besides, the reaction rate constants of C_3H_8+O(^{3}P)→C_3H_7+OH reaction are calculated using μVT method with high accuracy, and the quantum-tunneling effects are accounted for by the multidimensional small-curvature-tunneling transmission coefficient. The temperature range for the computed rate constants is from 298 K to 1000 K, and the obtained rate constants at 298, 939, 946, and 957 K are in very good agreement with the experimental results. Additionally, the calculated branching ratios of the title reaction at 593, 944, and 1130 K are also in good agreement with the experimental results. What's more, the isotope effects of C_3H_8+O(^{3}P) are calculated and discussed. Importantly, these calculations have revealed the hydrogen-abstraction mechanisms of propane, which would be helpful for a deeper under-

DOI:10.1063/1674-0068/29/cjcp1603042

standing of the combustion of hydrocarbon.

V. ACKNOWLEDGMENTS

This work is supported by the Chinese Ministry of Science and Technology (No.2013CB834601), and the National Natural Science Foundation of China (No.21303217 and No.21473218), and Institute of Chemistry, Chinese Academy of Sciences (No.20140160).

[1] K. J. Morganti, T. M. Foong, M. J. Brear, G. da Silva, Y. Yang, and F. L. Dryer, Fuel **108**, 797 (2013).
[2] N. C. Surawski, B. Miljevic, T. A. Bodisco, R. Situ, R. J. Brown, and Z. D. Ristovski, Fuel **133**, 17 (2014).
[3] A. G. McLain and C. J. Jachimowski, NASA Technical Note. D-8501 (1977).
[4] S. P. Jewell, K. A. Holbrook, and G. A. Oldershaw, Int. J. Chem. Kinet. **13**, 69 (1981).
[5] N. Cohen and K. R. Westberg, J. Phys. Chem. **20**, 1211 (1991).
[6] A. Miyoshi, K. Tsuchiya, N. Yamauchi, and H. Matsui, J. Phys. Chem. **98**, 11452 (1994).
[7] A. Miyoshi, N. Yamauchi, and H. Matsui, J. Phys. Chem. **100**, 4893 (1996).
[8] J. Zhang, L. Yang, and D. Troya, Chin. J. Chem. Phys. **26**, 765 (2013).
[9] D. Troya and G. C. Schatz, Theor. Chem. Rea. Dynam. **145**, 329 (2004).
[10] D. Troya, J. Phys. Chem A **111**, 10745 (2007).
[11] C. Gonzalez and H. B. Schlegel, J. Phys. Chem. **94**, 5523 (1990).
[12] K. Fukuil, J. Phys. Chem. **74**, 4161 (1970).
[13] H. Zhao, W. Bian, and K. Liu, J. Phys. Chem. A **110**, 7858 (2006).
[14] H. Zhao, L. Pan, and W. Bian, Int. J. Quantum. Chem. **112**, 858 (2012).
[15] H. Ma, C. Shi, W. Bian, H. Su, and F. Kong, Chin. J. Chem. Phys. **20**, 383 (2007).
[16] J. Cao, Z. Zhang, C. Zhang, W. Bian, and Y. Guo, J. Chem. Phys. **134**. 024315 (2011).
[17] M. J. Frisch, G. W. Trucks, H. B. Schlegel, G. E. Scuseria, M. A. Robb, J. R. Cheese-man, G. Scalmani, V. Barone, B. Mennucci, G. A. Petersson, H. Nakatsuji, M. Caricato, X. Li, H. P. Hratchian, A. F. Izmaylov, J. Bloino, G. Zheng, J. L. Sonnenberg, M. Hada, M. Ehara, K. Toyota, R. Fukuda, J. Hasegawa, M. Ishida, T. Nakajima,Y. Honda, O. Kitao, H. Nakai, T. Vreven, J. A. Montgomery Jr., J. E. Peralta, F. Ogliaro, M. Bearpark, J. J. Heyd, E. Brothers, K. N. Kudin, V. N. Staroverov, T. Keith, R. Kobayashi, J. Normand, K. Raghavachari, A. Rendell, J. C. Burant, S. S. Iyengar, J. Tomasi, M. Cossi, N. Rega, J. M. Millam, M. Klene, J. E. Knox, J. B. Cross, V. Bakken, C. Adamo, J. Jaramillo, R. Gomperts, R. E. Stratmann, O. Yazyev, A. J. Austin, R. Cammi, C. Pomelli, J. W. Ochterski, R. L. Martin, K. Morokuma, V. G. Zakrzewski, G. A. Voth, P. Salvador, J. J. Dannenberg, S. Dapprich, A. D. Daniels, Ö. Farkas, J. B. Foresman, J. V. Ortiz, J. Cioslowski, and D. J. Fox, *Gaussian 09*, Wallingford CT: Gaussian, Inc., (2010).
[18] J. Zheng, S. Zhang, B. J. Lynch, J. C. Corchado, Y. Y. Chuang, P. L. Fast, W. P. Hu, Y. P. Liu, G. C. Lynch, K. A. Nguyen, C. F. Jackels, A. Fernandez Ramos, B. A. Ellingson, V. S. Melissas, J. Villà, I. Rossi, E. L. Coitiño, J. Pu, T. V. Albu, A. Ratkiewicz, R. Steckler, B. C. Garrett, A. D. Isaacson, and D. G. Truhlar, *Polyrate, version 2015*, Minneapolis: University of Minnesota, (2015).
[19] Q. S. Li, J. Yang, and S. Zhang, J. Phys. Chem. A. **110**, 11113 (2006).
[20] H. Ma, X. Liu, W. Bian, L. Meng, and S. Zheng, ChemPhysChem. **7**, 1786 (2006).
[21] W. J. van Zeist, A. H. Koers, L. P. Wolters, and F. M. Bickelhaupt, J. Chem. Theory Comput. **4**, 920 (2008).
[22] X. Liu, W. Bian, X. Zhao, and X. Tao, J. Chem. Phys. **125**, 074306 (2006).
[23] D. Skouteris, D. E. Manolopoulos, W. Bian, H. J. Werner, L. H. Lai, and K. Liu, Science **286**, 1713 (1999).
[24] C. Zhang, M. Fu, Z. Shen, H. Ma, and W. Bian, J. Chem. Phys. **140**, 234301 (2014).
[25] J. Yu, S. Chen, and C. Yu, J. Chem. Phys. **118**, 582 (2003).
[26] A. Neugebauer and G. Häfelinger, Int. J. Mol. Sci. **6**, 157 (2005).
[27] K. G. M. Florian Ausfeldera, Prog. React. Kinet. Mech. **25**, 299 (2000).
[28] K. Ukui, Acc. Chem. Res. **14**, 363 (1981).
[29] K. Ishida, K. Morokuma, and A. Komornicki, J. Chem. Phys. **66**, 2153 (1977).
[30] X. Liu, M. A. MacDonald, and R. D. Coombe, J. Phys. Chem. **96**, 4907 (1992).
[31] T. H. R. Lowry, K. S Richardson, *Mechanism and Theory in Organic Chemistry*, New York: Harper and Row, 232 (1987).

DOI:10.1063/1674-0068/29/cjcp1603042